The impact of different aperture distribution models and critical stress criteria on equivalent permeability in fractured rocks

Bisdom, Kevin; Bertotti, Giovanni; Nick, Hamid

Published in:
Journal of Geophysical Research: Solid Earth

Link to article, DOI:
10.1002/2015JB012657

Publication date:
2016

Document Version
Publisher's PDF, also known as Version of record

AGU PUBLICATIONS

JGR

Journal of Geophysical Research: Solid Earth

RESEARCH ARTICLE
10.1002/2015JB012657

Key Points:
- The impact of three aperture definitions on equivalent permeability is compared, using large-scale realistic fracture network geometries
- The modeled apertures are heterogeneous along single fractures, resulting in a lower permeability compared to averaged constant apertures
- Hydraulically closed fracture segments are more controlling for flow in a low-permeability matrix than absolute aperture

Correspondence to:
K. Bisdom,
k.bisdom@tudelft.nl

Citation:
Bisdom, K., G. Bertotti, and H. M. Nick (2016), The impact of different aperture distribution models and critical stress criteria on equivalent permeability in fractured rocks, *J. Geophys. Res. Solid Earth*, *121*, 4045–4063, doi:10.1002/2015JB012657.

Received 13 NOV 2015
Accepted 7 MAY 2016
Accepted article online 13 MAY 2016
Published online 30 MAY 2016

The impact of different aperture distribution models and critical stress criteria on equivalent permeability in fractured rocks

Kevin Bisdom[1], Giovanni Bertotti[1], and Hamidreza M. Nick[1,2]

[1]Department of Geoscience and Engineering, Delft University of Technology, Delft, Netherlands, [2]The Danish Hydrocarbon Research and Technology Centre, Technical University of Denmark, Copenhagen, Denmark

Abstract Predicting equivalent permeability in fractured reservoirs requires an understanding of the fracture network geometry and apertures. There are different methods for defining aperture, based on outcrop observations (power law scaling), fundamental mechanics (sublinear length-aperture scaling), and experiments (Barton-Bandis conductive shearing). Each method predicts heterogeneous apertures, even along single fractures (i.e., intrafracture variations), but most fractured reservoir models imply constant apertures for single fractures. We compare the relative differences in aperture and permeability predicted by three aperture methods, where permeability is modeled in explicit fracture networks with coupled fracture-matrix flow. Aperture varies along single fractures, and geomechanical relations are used to identify which fractures are critically stressed. The aperture models are applied to real-world large-scale fracture networks. (Sub)linear length scaling predicts the largest average aperture and equivalent permeability. Barton-Bandis aperture is smaller, predicting on average a sixfold increase compared to matrix permeability. Application of critical stress criteria results in a decrease in the fraction of open fractures. For the applied stress conditions, Coulomb predicts that 50% of the network is critically stressed, compared to 80% for Barton-Bandis peak shear. The impact of the fracture network on equivalent permeability depends on the matrix hydraulic properties, as in a low-permeable matrix, intrafracture connectivity, i.e., the opening along a single fracture, controls equivalent permeability, whereas for a more permeable matrix, absolute apertures have a larger impact. Quantification of fracture flow regimes using only the ratio of fracture versus matrix permeability is insufficient, as these regimes also depend on aperture variations within fractures.

1. Introduction

Natural fractures may significantly impact subsurface fluid flow patterns, either positively or negatively [*Nelson*, 2001; *Narr et al*., 2006]. The contribution of flow through fractures to total reservoir flow is difficult to quantify, as it requires an understanding of the 3-D fracture network geometry, including length, spacing, orientation, and aperture distributions. Integrated studies combining outcrops with well data and seismic attributes provide constraints for most fracture geometrical parameters, as well as rules to extrapolate 1-D well data to reservoir-scale fracture models based on geomechanical relations or seismic attributes, provided that the data are accurately captured and corrected for sampling artifacts [*Narr*, 1996; *Wu and Pollard*, 2002; *Narr et al*., 2006; *Ortega et al*., 2006; *Makel*, 2007].

Fracture aperture is less commonly analyzed, resulting in large uncertainties in fluid flow modeling, as small variations in aperture have large implications on rock flow [*de Dreuzy et al*., 2001, 2002, 2012; *Matthäi and Belayneh*, 2004; *Klimczak et al*., 2010; *Schultz et al*., 2013] and transport properties [*Nick et al*., 2011]. Borehole imaging tools provide an estimate of aperture [*Luthi and Souhaite*, 1990], although with some uncertainty, especially in the absence of accurate calibration [*Makel*, 2007; *Ponziani et al*., 2015].

In outcrops, veins may be used to quantify kinematic opening, but outcrops with large numbers of veins covering a range of scales are rare, and barren fractures are not representative as exhumation and weathering may open previously cemented or closed fractures [e.g., *Gale et al*., 2014]. Furthermore, outcropping apertures do not take into account the impact of in situ stresses.

Alternatively, models based on Linear Elastic Fracture Mechanics (LEFM) [*Lawn and Wilshaw*, 1975; *Segall*, 1984; *Pollard and Segall*, 1987; *Olson*, 2003] or experimental analysis of rock joints are used to predict aperture at reservoir stress conditions [*Barton*, 1982; *Bandis et al*., 1983; *Barton et al*., 1985], resulting in a range of distributions,

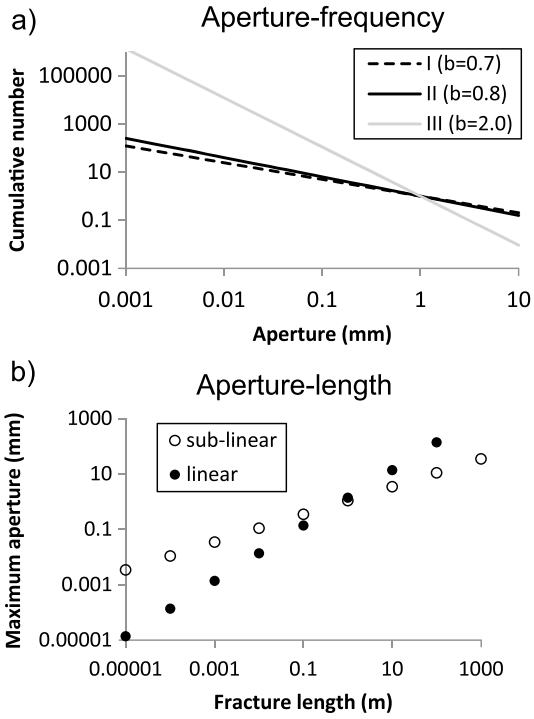

Figure 1. Commonly used aperture distributions derived from outcrop data and LEFM relations: (a) Aperture-frequency power law scaling relations for different power law exponents and (b) linear and sublinear length-aperture scaling relations.

depending on which method is used. The impact of each method on fluid flow in fractures has been studied extensively [e.g., *Baghbanan and Jing*, 2008; *Lei et al*., 2014; *Moos and Barton*, 2008; *Tao et al*., 2009]. In particular, the impact of power law aperture scaling and similar statistical distributions on permeability has been studied in 2-D and 3-D [*de Dreuzy et al*., 2001, 2002, 2012]. However, there is no direct comparison between the fundamentally different LEFM, Barton-Bandis and power law scaling methods, and their impact on equivalent (i.e., combined matrix and fracture) permeability in large-scale natural fracture networks.

The aim of this study is to compare the different aperture models and their impact on equivalent permeability in naturally fractured reservoirs, using equivalent permeability models [e.g., *Matthäi and Belayneh*, 2004]. We consider different critical stress criteria to predict which fractures will contribute to fluid flow under in situ stress conditions. We quantify the differences by applying each method to a series of realistic fracture networks, i.e., deterministic patterns digitized from outcropping carbonate and sandstone pavements, that include spatial variations and curved fracture shapes that are not fully considered in stochastic models. These models provide an improved understanding of the relative impact of fracture flow on equivalent permeability as a function of aperture definitions and matrix permeability.

2. Methodology

2.1. Models for Aperture Prediction

We focus on kinematic aperture, i.e., the opening between two subparallel fracture walls [*Marrett et al*., 1999], without considering if the intervening space is void or partially or fully cemented. For brevity, this is referred to as "aperture" in this study. We consider three different models: (i) power law scaling derived from vein measurements, (ii) opening displacement defined by LEFM subcritical crack growth, and (iii) the Barton-Bandis model for shear-induced dilation.

2.1.1. Aperture-Frequency Scaling Derived From Vein Analysis

A number of systematic studies on outcropping veins have documented that aperture follows power law frequency scaling, defined by the probability density function:

$$F = aX^{-b} \tag{1}$$

where F is the frequency for aperture X (in m), b is the power law exponent, and a is a fracture network density constant [*Bonnet et al*., 2001; *Ortega et al*., 2006; *Hooker et al*., 2012, 2013, 2014]. In sandstones, aperture scaling may be described by a universal exponent [*Hooker et al*., 2014], whereas for carbonates variable exponents are inferred [*Hooker et al*., 2012, and references therein]. These different values are likely related to trends in lithology or mechanical units, which may constrain the growth of fractures, but no physical relation between these outcrop properties and scaling exponents has been observed [*Odling et al*., 1999; *Bonnet et al*., 2001; *Hooker et al*., 2012].

The relation between the aperture-frequency distribution and other fracture geometrical parameters is generally not quantified in outcrop studies, and hence, the resulting distributions are randomly applied to fractures in Discrete Fracture Network (DFN) reservoir models. Although some studies note that vein

thickness may scale with length [*Olson*, 2003; *Hooker et al*., 2012], there is little explicit evidence derived from outcropping veins. We model aperture-frequency distributions by assigning apertures independent from fracture geometry using power law exponents of 0.8 (the universal scaling exponent for apertures in sandstones), 0.7, and 2.0 (common values found for carbonate rocks; Figure 1a) [*Hooker et al*., 2014, and references therein].

2.1.2. Fracture Opening Predicted by Linear Elastic Fracture Mechanics

LEFM describes a single phase of opening as a function of stress [*Lawn and Wilshaw*, 1975], where the maximum displacement $d_{\max}$ (in m) in the direction perpendicular to the fracture walls is defined by

$$d_{\max} = \frac{K_C(1-\nu^2)}{E\sqrt{\frac{\pi}{8}}}\sqrt{L} \tag{2}$$

where ν and E are the Poisson's ratio and Young's modulus (in Pa), L is fracture length (in m), and K_c is the fracture toughness, defined as $K_C = \Delta\sigma_l\sqrt{\pi L/2}$. $\Delta\sigma_l$ is the driving stress (in Pa), which is the difference between fluid pressure P_f within the fracture and normal stress σ_n acting on the fracture [*Lawn and Wilshaw*, 1975; *Pollard and Segall*, 1987; *Vermilye and Scholz*, 1995; *Olson*, 2003; *Anders et al*., 2014]. Critical crack growth occurs when $P_f > \sigma_n$, i.e., when hydraulic fracturing takes place [*Segall*, 1984; *Engelder and Lacazette*, 1990]. This stress condition is, however, relatively rare in most subsurface rocks and does not explain the abundance of open natural fractures [*Atkinson*, 1984; *Segall*, 1984; *Lorenz et al*., 1991; *Swarbrick et al*., 2002].

Opening of natural fractures in the subsurface under relatively low fluid pressure may be more accurately described by subcritical crack growth, which states that over longer (i.e., geological) time scales, opening occurs in small increments when a subcritical toughness criterion is reached [*Segall and Pollard*, 1983]. The subcritical toughness is generally defined as $K_C^* \cong K_C/10$ [*Atkinson*, 1984; *Segall*, 1984; *Olson et al*., 2009].

The behavior of fracture toughness with respect to length defined by equation (2) is matter of debate, as K_c is either considered to scale linearly with length on all scales, or only for small fractures [*Olson*, 2003; *Scholz*, 2010, 2011; *Olson and Schultz*, 2011; *Anders et al*., 2014]. In the case of a constant K_C^*, aperture scales with the square root of length (i.e., sublinear) instead of linearly [*Olson*, 2003]. Depending on the chosen parameters used to define the scaling behavior, the linear and sublinear trends may intersect. We apply both submethods, using constant mechanical rock properties and stress conditions, and quantify the differences in terms of aperture and flow. For the applied parameters, the sublinear method predicts smaller apertures for fractures longer than 1 m and larger apertures for fractures shorter than 1 m, compared to linear scaling (Figure 1b).

2.1.3. Shear-Induced Dilation in Poorly Interlocking Fractures

Observations from outcrops show that fractures are typically characterized by irregular fracture walls with some shear displacement and a nonelliptical aperture, which does not correspond to the ellipse shape predicted by LEFM. For these fractures, the Barton-Bandis model can be used to predict the aperture of a fracture with irregular walls that experiences some shear under compression [*Barton and Bandis*, 1980; *Barton*, 1982]. The mismatched fracture walls lead to an aperture that is quantified using a set of empirical functions based on normal stress and shear displacement [*Barton*, 1982, 2014; *Bandis et al*., 1983; *Barton et al*., 1985].

The stress-dependent aperture E_n (in mm) is defined as a hyperbolic function of the driving stress $\Delta\sigma_l$ (in MPa):

$$E_n = E_0 - \left(\frac{1}{v_m} + \frac{K_{ni}}{\Delta\sigma_l}\right)^{-1} \tag{3}$$

where E_0 is the initial unstressed aperture (in mm), which is a function of fracture stiffness and roughness:

$$E_0 = \frac{\mathrm{JRC}}{5}\left(0.2\frac{\sigma_c}{\mathrm{JCS}} - 0.1\right) \tag{4}$$

where σ_c is the uniaxial compressive strength (in MPa), JRC is the dimensionless Joint Roughness Coefficient, derived from the irregularity of the fracture walls, and JCS is the Joint Compressive Strength (in MPa) [*Barton and Bandis*, 1980; *Barton et al*., 1985]. For an unweathered fracture, JCS equals σ_c such that E_0 is only a function of roughness. The JRC is either defined as the slip angle of a rock sample, measured using the fracture amplitude-length ratio or estimated using roughness profile matching [*Barton*, 2014]. Throughout this study, we assume irregular rough fractures (JRC = 15), resulting in an initial unstressed aperture of 0.3 mm that is

independent of length or network geometry [*Barton*, 2014; *Lei et al*., 2014; *Bisdom et al*., 2016a]. Maximum closure v_m (in mm) is the difference between maximum opening and the smallest aperture, and K_{ni} (in MPa/mm) is the initial fracture stiffness [*Bandis et al*., 1983]:

$$v_m = -0.1032 - 0.0074\text{JRC} + 1.135\left(\frac{\text{JCS}}{E_0}\right)^{-0.251} \tag{5}$$

$$K_{ni} = -7.15 + 1.75\text{JRC} + 0.02\frac{\text{JCS}}{E_0} \tag{6}$$

2.2. Models for Critically Stressed Fractures

The described models capture the kinematic aperture, but this is not directly representative of the actual flow through a fracture network, as analysis of subsurface data indicates that not all fractures contribute to flow. In an impermeable matrix, dead ends of fractures have no impact on flow, such that only the backbone of the network should be considered [*Odling et al*., 1999]. However, even within the backbone, only part of the network is assumed hydraulically open depending on whether fractures are critically stressed [*Barton et al*., 1995; *Rogers*, 2003]. We consider two critical stress definitions, the Coulomb friction criterion and the Barton-Bandis peak shear criterion.

The Coulomb criterion depends on the stress magnitude and the orientation of the fracture in the in situ heterogeneous stress field. The orientation impacts the normal and shear stresses on the fracture plane. When shear stress exceeds shear stiffness, shearing causes dilation that keeps the fracture hydraulically open [*Rogers*, 2003]. Fractures in this stress state are referred to as reactivated or critically stressed [*Barton et al*., 1995; *Rogers*, 2003]. We use this definition to define critically stressed fractures derived from the power law scaling distribution and subcritical crack growth model.

The Barton-Bandis model uses a different definition for hydraulically open fractures, defined by the ratio between the shear displacement and a peak shear displacement, which is an implicit function of orientation, size, and spacing [*Olsson and Barton*, 2001; *Baghbanan and Jing*, 2008]. We only consider the relation between stress and hydraulically open fractures; i.e., we do not consider the role of cement bridges in keeping fractures open [*Laubach et al*., 2004; *Philip et al*., 2005; *Hooker et al*., 2012].

2.2.1. Coulomb Friction

The friction curve is defined by $\tau = \mu(\sigma_n - P_f)$ where μ is the surface friction coefficient. This coefficient is generally found to be 0.6 [*Rogers*, 2003], which is the value used in this study. We assume a σ_1 of 30 MPa, oriented N-S (i.e., 0° azimuth) and a σ_3 of 10 MPa. For these stresses, Mohr-Coulomb predicts that fractures with a strike between 9° and 51° are critically stressed. This approach, although simplistic, is widely used to model fracture aperture in subsurface models [*Barton et al*., 1995; *Zoback*, 2007].

2.2.2. Barton-Bandis Peak Shearing

Quantification of flow through critically stressed fractures in the Barton-Bandis model is defined by a hydraulic aperture, which is approximately equal to the physical opening when a fracture is critically stressed, but close to zero for noncritically stressed fractures [*Olsson and Barton*, 2001]. Hydraulic aperture is defined by the ratio between shear displacement and a peak shear displacement u_{peak} (in m):

$$u_{\text{peak}} = \frac{B_n}{500}\left[\frac{\text{JRC}_n}{B_n}\right]^{0.33} \tag{7}$$

where B_n is the block size (in m) and JRC_n is the corresponding JRC of each fracture segment n [*Barton*, 1982]. The block size is the spacing of the fracture set that intersects the fracture of interest [*Barton*, 1982]. Shear displacement is obtained from numerical models, but an approximation of shear displacement u_{geom} for the parameters used in this study can be obtained from a geometrical function that is dependent on block size, far-field stresses, and the orientation of the fracture with respect to the far-field stresses [*Bisdom et al*., 2016a]:

$$u_{\text{geom}} = B_n.\sigma_n.\alpha\left(-9.07{\cdot}10^{-8}\alpha + 8.1{\cdot}10^{-6}\right) \tag{8}$$

The ratio between u_{geom} and u_{peak} defines whether the fracture is critically stressed:

$$e = \begin{cases} \dfrac{E_n^2}{\text{JRC}^{2.5}} & \text{for} \dfrac{u_{\text{geom}}}{u_{\text{peak}}} \leq 0.75 \\ \sqrt{E_n \text{JRC}_{\text{mob}}} & \text{for} \dfrac{u_{\text{geom}}}{u_{\text{peak}}} \geq 1 \end{cases} \tag{9}$$

where e is hydraulic aperture in mm [*Olsson and Barton*, 2001]. For $0.75 \leq u_s/u_{peak} \leq 1$, e is interpolated linearly [*Olsson and Barton*, 2001]. When shear displacement is larger than peak shear displacement, the fracture is critically stressed. However, even when shear displacement is less than peak shear displacement, the fracture may still provide a small contribution to flow from an aperture resulting from a mismatch between fracture walls [*Barton*, 2014].

2.3. Equivalent Permeability Modeling

The impact of critically stressed aperture on fluid flow is quantified using equivalent permeability, which considers matrix and fracture flow and the interaction between the two. The fracture geometry and heterogeneous aperture distribution are not upscaled [*Matthäi et al*., 2009]. Fracture permeability (in m^2) is calculated from hydraulic aperture e (in m) assuming laminar flow between two parallel plates using $k_f = e^2/12$, calculated for each linear fracture segment [*Snow*, 1969].

Equivalent permeability is calculated utilizing a Finite Element Finite-Volume (FEFV) approach in which the steady state continuity equation for flow $\nabla \cdot q = 0$ is solved, where q is the Darcy velocity $q = -k\nabla p/\mu$ (in m/s), with pressure p in Pa, viscosity μ in Pa s, and intrinsic permeability k in m^2 [*Matthäi et al*., 2007]. The rock matrix is discretized by 2-D triangulated elements, and fractures are discretized using 1-D line elements. Depending on model size and fracture intensity, the mesh size varies between 3×10^5 and 1×10^6 elements. The mesh is refined to a resolution of 0.1 m around the fractures. This approach is implemented into the Complex System Modeling Platform (CSMP++), where a far-field pressure gradient of 10 kPa is applied in both horizontal directions of the rectangular 2-D pavements, after which the continuity equation is solved [*Paluszny and Matthäi*, 2010; *Nick and Matthäi*, 2011]. The meshing and flow modeling approach is discussed further in *Bisdom et al*. [2016b].

Similar to *Matthäi and Nick* [2009], the fluid flux across the model boundaries in the x and y directions is integrated and from this equivalent permeability is calculated using Darcy flow. Equivalent permeability is used to quantify fluid pressure for different aperture and matrix contrasts. Note that unlike *Lang et al*. [2014], we do not calculate the maximum permeability and corresponding permeability tensor but instead calculate permeability in the fixed x and y directions of the models, as we focus on characterizing the differences resulting from the different aperture models, rather than trying to predict maximum permeability. For brevity, we use "permeability" for equivalent permeability. When referring to matrix or intrinsic fracture permeability, it is stated explicitly.

2.4. Application to Realistic Multiscale Fracture Networks

2.4.1. Outcrop Data Set

The aperture and critical stress models are applied to seven deterministic fracture networks. Each of these networks has a unique spatial distribution and subsequent network connectivity, and the collection covers typically observed fracture patterns. These data sets, although they are deterministic and cover in most cases large areas with a relatively high resolution, still suffer from limited sampling and truncation artifacts.

Five data sets were obtained from carbonate pavements located in Brazil, which we refer to as "*Brazil I*" to "*Brazil V*" [*Bertotti and Bisdom*, 2013]. These pavements are part of a subhorizontal postrift carbonate sequence (the Albian Jandaíra Formation), deposited in the Potiguar basin in northeast Brazil [*Reis et al*., 2013]. Although these pavements are located in the same structural domain, they display fracture networks with different spatial distributions. Brazil I consists of three mutually cross-cutting orientation families with power law length scaling. Brazil II shows conjugate fractures with a small conjugate angle. Brazil III is representative of multiscale networks where smaller fractures abut against larger fractures. The last two Brazil models (IV and V) are partially overlapping regions from one outcrop that contains a single N-S striking orientation set.

The sixth pavement was digitized from images in a steep flank of the Alima anticline (South Atlasic Fold Belt, central Tunisia) [*Bisdom*, 2015]. This pavement, characterized by two orthogonal sets of fractures with a relatively constant length, is part of the Eocene Kef Eddour Formation [*Riley et al*., 2010]. For the purpose of this study, we rotated back the data to its prefolding horizontal position, as the fractures were created during burial, prior to folding. The last data set was obtained from Devonian sandstones outcropping in a gently dipping fold in the Anti-Atlas of Morocco [*Guiton et al*., 2003]. This pavement contains two long orthogonal sets and an oblique set that abuts against the larger systems and is comparable to high-intensity systems such as the Bristol Channel [*Belayneh et al*., 2006]. All pavements have in common that the majority of

Journal of Geophysical Research: Solid Earth

10.1002/2015JB012657

Table 1. Summary of Fracture Statistics for Each Fracture Pavement[a]

Pavement Name	Formation and Location (Latitude/Longitude)	Rock Type, Age, and Formation Name	Fracturing	Spatial Distribution	Number of Fractures	Average Length and Length Range (m)	Censoring/ Truncation Limits (m)	Average P_{21} (m^{-1})	Intersections/ Density	Network Saturation (%)
Tunisia	Gafsa basin, Central Tunisia (34.335626, 8.330545)	Eocene Kef Eddour Formation (carbonates)	Bed-perpendicular conjugate fractures	Two perpendicular systems (N-S and E-W)	345	11.8 (1.0–53.0 m)	3.5–53	0.22	1.3	42%
Morocco	Anti-Atlas, Morocco (29.576328, −7.983062)	Devonian Rich Formation (sandstones)	Bed-perpendicular orthogonal fracturing with three orientation sets	Hierarchical fracture systems with homogeneous spacing	1706	3.7 (0.4–44.0 m)	0.5–44	2.55	5.8	97%
Brazil I	Jandaira Formation, Potiguar basin, NE Brazil (−5.5610578, −37.661895)	Upper Cretaceous Jandaira Formation (carbonates)	Bed-perpendicular conjugates and joints	Three orientation families with a wide scatter in size and orientation	358	21.8 (3.4–218.0 m)	4.0–218.0	0.12	2.0	80%
Brazil II	(−5.536467, −37.639803)			One large system (N-S) and locally small E-W fractures	644	20.0 (1.2–123.0 m)	4.0–123.0	0.31	0.9	23%
Brazil III	(−5.495950, −37.549517)			Fractal system with chaotic orientations	791	5.8 (0.2–53.1 m)	2.0–53.1	0.29	1.7	68%
Brazil IV	(−5.515234, −37.611794)		Bed-perpendicular joints	One system with few intersections, striking NNE-SSW	236	0.9 (0.1–6.7 m)	0.2–6.7	1.30	0.1	2%

[a] P_{21} is a measure of fracture intensity, defined as the total length of fractures $\sum l$ within a given area of outcrop A: $\sum l/A$ [*Dershowitz and Einstein*, 1988]. The percolation probability is defined using normalized intersections as a function of density as defined by [*Robinson*, 1983] and by using the network saturation.

fractures are the result of regional shortening in subhorizontal layers, creating bed-perpendicular fractures, with limited fold-related fractures in the Morocco model [*Guiton et al.*, 2003; *Bertotti et al.*, 2013].

The varying spatial and size distributions result in a fracture network connectivity that is different in each pavement. As these differences will impact permeability independent from variations in the aperture distribution, we quantify connectivity using two percolation parameters (Table 1). The first parameter is the commonly used percolation probability defined by fracture density and the number of intersections, normalized by the outcrop area [*Robinson*, 1983, 1984]. However, as this method does not fully consider fracture length, we also perform a cluster analysis, where the percolation probability is a function of the area of rock covered by a connected network versus total outcrop area [*Berkowitz and Balberg*, 1993; *Berkowitz*, 1995].

All pavements were imaged using the md4-200 quadcopter (Microdrones GmbH), an Unmanned Aerial Vehicle (UAV or "drone") equipped with a compact camera. Using photogrammetry, the images were merged into high-resolution georeferenced orthophotos, on which the fractures were digitized using DigiFract software [*Hardebol and Bertotti*, 2013]. The orthophotos have a resolution of at least 1 cm per pixel and cover uncensored areas of outcropping fracture networks of up to 3×10^5 m^2, resulting in less censoring and truncation artifacts than most other networks reported in literature. As the studied networks have similar resolutions and dimensions, we can compare length and spacing trends between different pavements [*Ortega et al.*, 2006]. The geometrical and spatial characteristics of the fracture networks are summarized in Table 1.

2.4.2. Model Boundary Conditions

We compare three aperture methods with in total six submodels that are applied to the fracture networks: (1) power law frequency scaling with three commonly observed exponents (0.7, 0.8, and 2.0), (2) two variations of LEFM aperture scaling (linear and sublinear), and (3) Barton-Bandis conductive shearing.

The driving stress required for the length-aperture and Barton-Bandis models is a function of normal stress and fluid pressure. Normal stress is calculated using $\sigma_n = 0.5(\sigma_1 + \sigma_3) + 0.5(\sigma_1 + \sigma_3)\cos 2\beta$ where σ_1 and σ_3 are the maximum and minimum horizontal stresses in a horizontal plane-strain cross section of the fracture network [e.g., *Zoback*, 2007]. The angle β is the angle between the fracture and σ_1 [*Zoback*, 2007]. In all models, σ_1 is 30 MPa with a 0° azimuth and the Poisson's ratio is 0.3, resulting in a σ_3 of 10 MPa (i.e., Poisson's stress). Fluid pressure is constant; i.e., we do not consider short-term changes in pressure during production.

This definition of σ_n does not consider local stress perturbations related to fracture geometry, except for orientation. Solving for local stresses requires more robust approaches, such as finite element models [*Lei et al.*, 2014, 2015; *Bisdom et al.*, 2016a, 2016b]. Assuming that the far-field stress equals local stress is a simplification that may overestimate absolute aperture. For the Barton-Bandis model, aperture is up to 5% higher for far-field stress, compared to a local stress distribution modeled using finite element simulations [*Bisdom et al.*, 2016a]. However, our aim is to compare relative aperture and permeability trends, for which we make the assumption that far-field stress is representative of local stress. As a result of this simplification, as well as the omission of the role of cement during fracture development [*Philip et al.*, 2005; *Laubach and Ward*, 2006], the absolute aperture values presented are likely an overestimation of true 2-D aperture.

After calculating aperture for each model, we quantify the fraction of the network that is critically stressed under a N-S maximum horizontal stress, using the ratio between shear displacement and peak shear displacement in the Barton-Bandis peak shearing model and the Coulomb stress state in the other models.

3. Aperture Results

We first present the results for initial aperture, which does not consider the impact of critical stress criteria, to quantify aperture for the entire network where all fractures have an aperture larger than zero. By comparing initial aperture to the critically stressed distribution, we aim to show the impact of critical stress criteria.

3.1. Initial Noncritically Stressed Aperture

3.1.1. Outcrop-Based Power Law Frequency Scaling

As power law scaling is independent of geometry, the resulting aperture is only a function of the scaling exponent, where a higher exponent results in more small values (Figure 2a). The length-weighted average decreases for increasing exponents (Figure 2b). There is some scatter in average aperture between the different pavements,

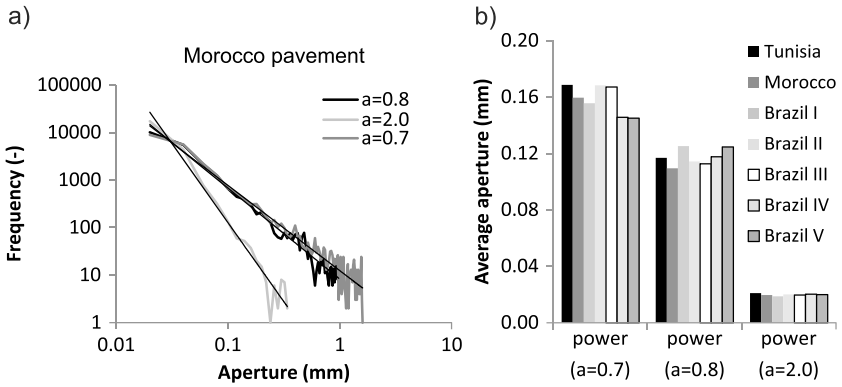

Figure 2. Power law scaling aperture distributions: (a) frequency distributions for the three different power law exponents, calculated for the *Morocco* pavement and (b) average length-weighted aperture per pavement for each of the power law scaling exponents.

as it is assigned randomly, creating a heterogeneous distribution (Figure 3). However, the majority of fractures has small apertures, i.e., less than 0.1 mm, whereas only a small subset has relatively large values of up to 10 mm.

3.1.2. (Sub)linear Length Scaling

Linear length-aperture scaling predicts apertures ranging from micron-scale to more than 50 mm, with some more extreme values, depending on fracture length (Figure 4a). Sublinear aperture scaling ranges from micron-scale to several millimeters. The length-weighted average is largest for the pavements with the largest average fracture lengths, i.e., Brazil I and Brazil II (Table 1 and Figure 4b). However, these are also the largest outcrop models, and the length and aperture distributions in Brazil I are skewed because of a single 200 m long N-S trending fracture. As average aperture is partly dependent on outcrop size, the complete aperture distribution may be more representative, as it shows the wide scatter, as well as the impact of a small set of very large fractures (Figure 5).

3.1.3. Barton-Bandis

Apertures predicted adopting the Barton-Bandis model for the specific boundary conditions of our experiment are between 0.17 and 0.21 mm (Figures 6a and 7). As normal aperture defined by equation (3) is primarily a function of stress rather than fracture geometry, it is the orientation between the fracture and σ_1 that has the largest impact. Pavements with fractures that strike at a small angle relative to σ_1 have the largest average aperture, even if lengths are small and spacing is high (Figure 6b).

For pavements that have uniform orientation sets, the aperture frequency distribution shows clear peaks corresponding to each set, whereas in pavements with a single orientation set, one peak is observed (Figure 6a).

3.1.4. Comparison of Aperture Distributions

Although aperture-frequency scaling results in some large apertures, most fractures have small values (i.e., less than 0.1 mm) and the subsequent average is smaller compared to the other methods (Figure 2b versus Figures 4b and 6b). For small exponents, the average of aperture-frequency scaling is close to that of the Barton-Bandis model (Figures 2b and 6b). However, the average of a power law function may not be representative, as a few extremely large values skew the distribution. In contrast, Barton-Bandis aperture is confined to a narrower domain, limited in between the initial aperture and the maximum closing (Figure 6a).

As fractures in the studied outcrops are relatively long, i.e., typically exceeding 1 m, aperture is larger for linear scaling compared to sublinear scaling. Depending on the pavement geometry, sublinear aperture is two to eight times smaller than linear aperture (Figure 4b). This difference is largest for the pavements with the largest average fracture length (i.e., Brazil I–II) and smallest for the pavements with relatively small fractures (Brazil IV–V). The aperture predicted by the (sub)linear methods is comparable to the other methods only for fractures shorter than 1 m.

3.2. Critically Stressed Aperture Distributions

For the applied far-field stress conditions, application of the Coulomb criterion to the (sub)linear length-aperture and power law frequency models results in the hydraulic closing of all fractures that are not within the critically stressed orientation domain of 9–51°. On average, this results in closing of 50% of the fracture

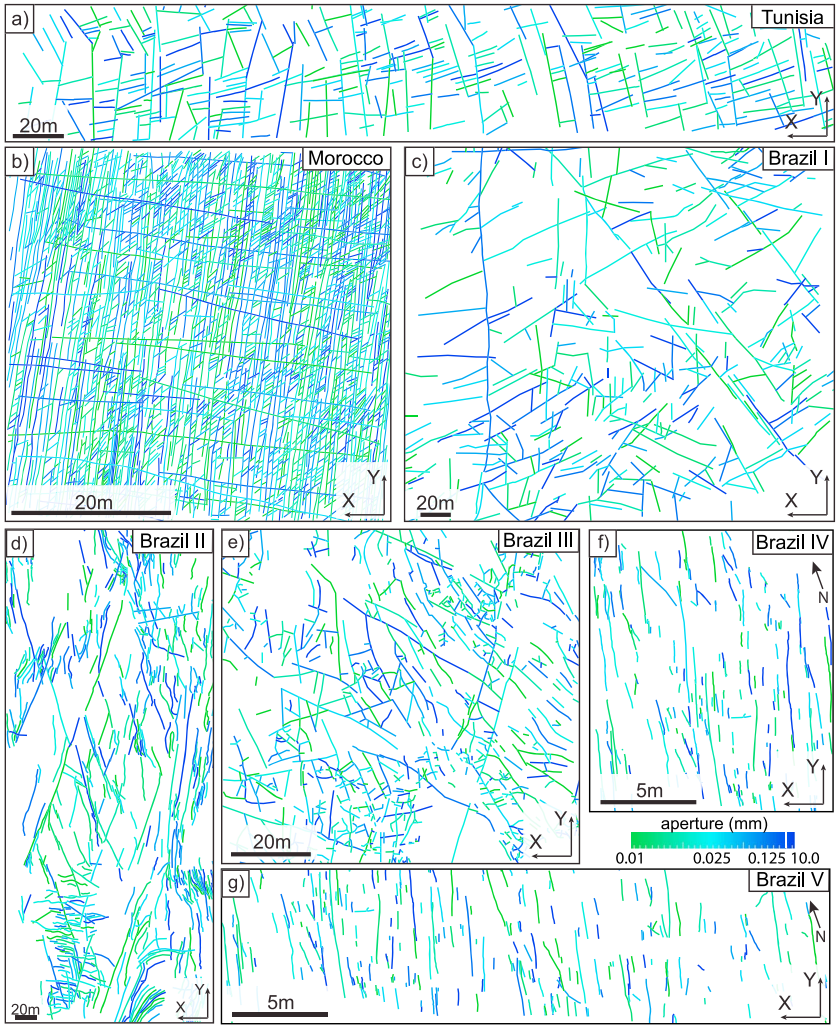

Figure 3. Fracture geometry and aperture distribution (in mm, note the nonlinear scale) for a power law exponent of 0.8 for all pavement models. North is directed up in all models except for Brazil IV/V. The *x* and *y* axes indicate the directions in which equivalent permeability is calculated. Fracture statistics for each pavement are listed in Table 1.

network (Table 2). This does not, however, lead to a 50% reduction of average aperture. The (sub)linear length-aperture models are a function of normal stress, where for equal fracture lengths, aperture is larger when a fracture is subparallel to σ_1. Applying the Coulomb criterion with the same σ_1 orientation as used for modeling, the initial aperture distribution results in closing of the largest apertures, resulting in an 85% decrease in aperture (Table 2).

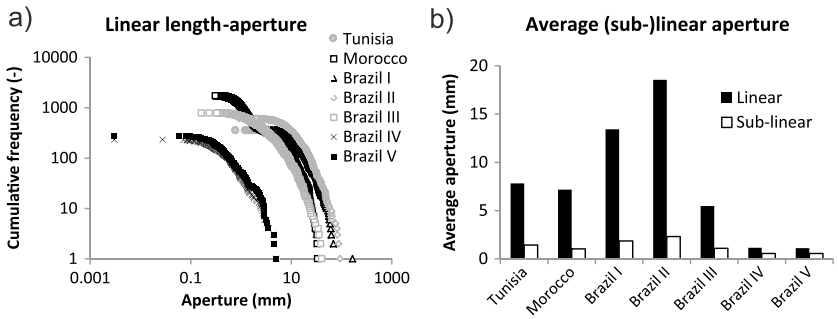

Figure 4. (Sub)linear length-aperture distributions: (a) cumulative frequency distributions for linear length-aperture of all pavements; (b) average length-weighted aperture per pavement for the (sub)linear aperture methods.

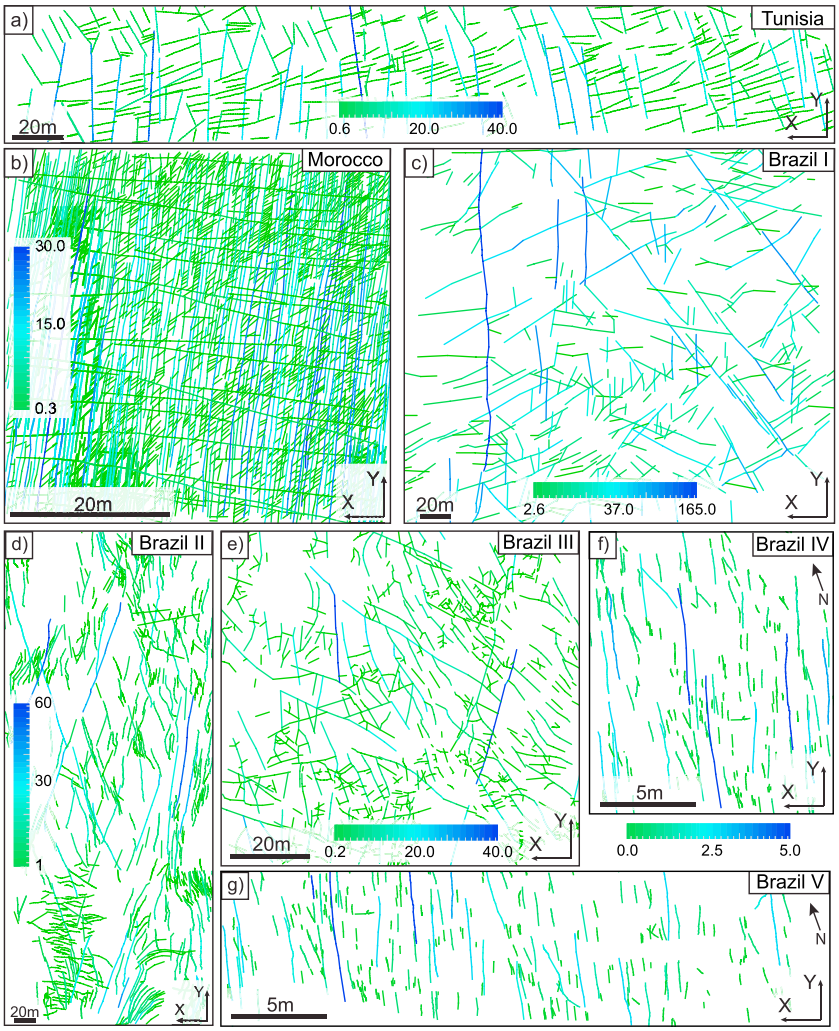

Figure 5. (a–g) Aperture distribution in each pavement, plotted for the linear length-aperture relation. Scale is indicated in mm, and absolute values vary per pavement. The scale bar between Figures 5f and 5g applies to both Brazil IV–V.

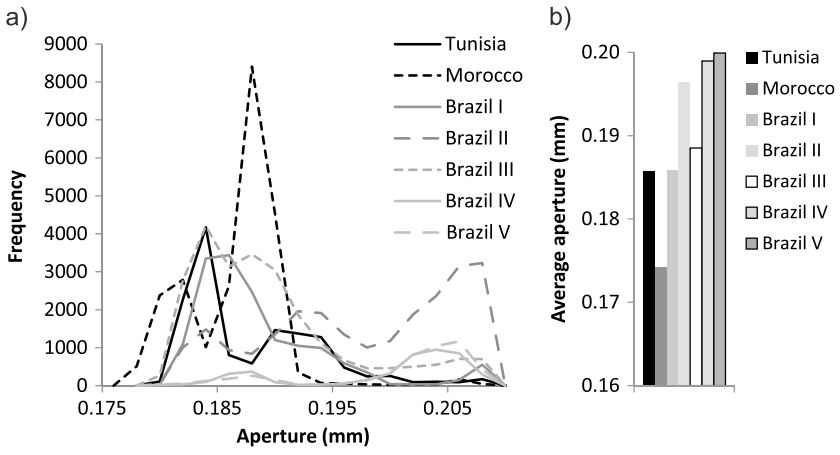

Figure 6. Fracture aperture distribution for the Barton-Bandis aperture method: (a) Aperture frequency distributions for all pavements; (b) average length-weighted aperture per pavement.

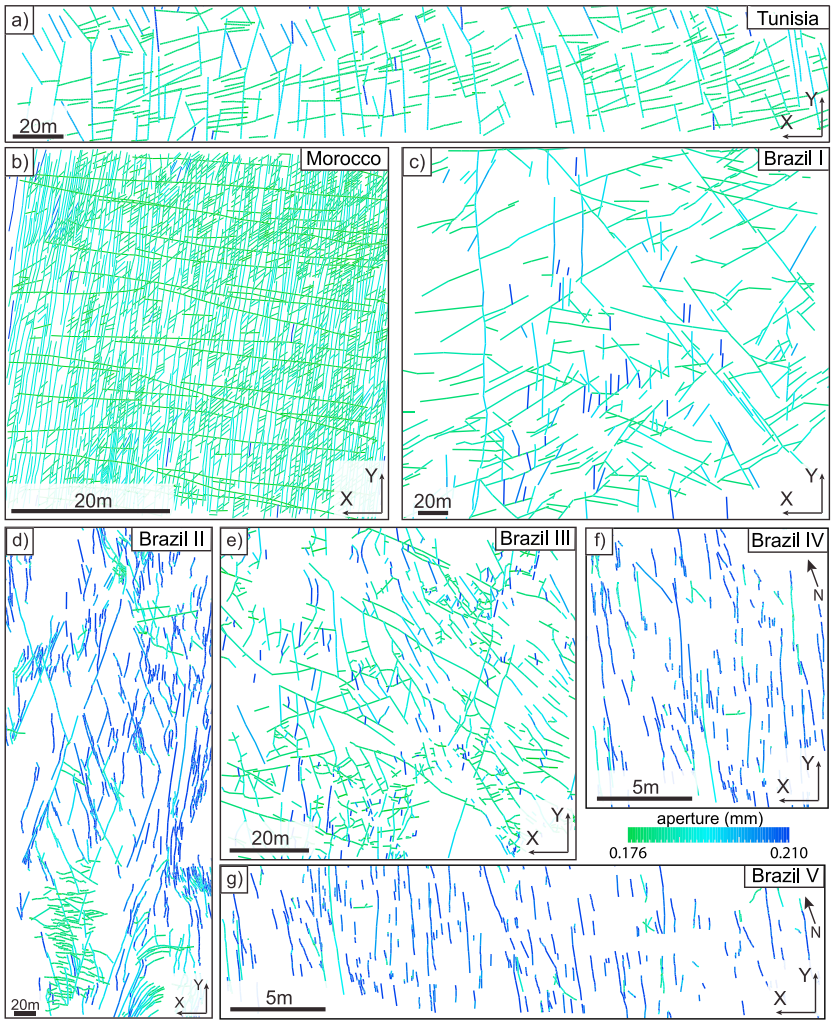

Figure 7. Barton-Bandis aperture distribution for all pavements.

For the Barton-Bandis model, peak shear and shear displacement in equation (9) are functions of orientation and block size, where a larger block size increases the probability of a fracture being critically stressed. As fractures are relatively large in most outcrops, with few intersections, the fraction of critically stressed fractures exceeds 80% for all models except the Morocco pavement (Table 2). In the Morocco pavement, the high number of fracture intersections results in small block sizes and a high fraction of closed fractures.

The difference between peak shearing and Coulomb is the result of the nonlinear behavior that is taken into account in the Barton-Bandis peak shear method [*Barton*, 2014]. This method is foremost a function of orientation with respect to σ_1, similar to Coulomb, but it also considers the fracture geometry, where a large block size increases the likelihood for a fracture to become critically stressed through equation (7). Furthermore, the peak shearing method assumes a transition between the open and closed domains defined in equation (9), whereas the Coulomb criterion only defines the two discrete domains, resulting in fractures that are partially hydraulically open in the Barton-Bandis model, whereas Coulomb considers them closed.

4. Permeability Results

4.1. Constant Matrix Permeability

Permeability is modeled for the six aperture methods applied to seven pavements, resulting in 42 simulations (Table 2). The full critically stressed aperture distribution, fluid pressure field, and fluid velocity are illustrated for one pavement (Figure 8). Matrix permeability in these models is constant (10 mD).

Table 2. Overview of Critically Stressed Fracture Aperture, Averaged for All Pavements, With the Average Absolute Aperture and the Percentage of Critically Stressed Fractures

	Coulomb					Peak Shear
Aperture Method	Power ($a = 2.0$)	Power ($a = 0.7$)	Power ($a = 0.8$)	Linear	Sublinear	Barton-Bandis
Ratio critically stressed fractures (-)						
Average	51%	48%	50%	50%	52%	78%
SD	20%	19%	18%	21%	20%	19%
Critically stressed aperture (mm)						
Average	0.01	0.08	0.06	5.22	0.29	0.15
SD	0.004	0.03	0.02	4.89	0.16	0.04
Equivalent permeability (critically stressed fractures)						
x (mD)	10.0	10.5	10.4	12.8	12.7	15.7
y (mD)	10.2	12.8	12.1	22.3	22.0	24.1
Anisotropy (-)	1.0	1.2	1.2	1.7	1.7	1.5
Equivalent permeability (all fractures)						
x (mD)	10.2	15.0	10.4	80,504.1	1,398.8	50.5
y (mD)	10.5	22.4	20.8	92,190.7	988.0	64.2
Anisotropy (-)	1.0	1.5	2.0	1.1	0.7	1.3
Critically stressed permeability ratio	1.0	1.6	1.4	4,917.2	68.7	2.9

4.1.1. Coulomb Criterion

The contribution of fracture permeability is small in critically stressed networks derived from the outcrop-based aperture-frequency distributions (Figure 8d). Permeability is highest in the y direction because of anisotropy related to network geometry and the orientation of σ_1. In the x direction, the impact of fractures on flow is negligible. This trend is found in all pavements, resulting in an overall low permeability (Table 2). The impact of fractures on permeability decreases for increasing power law exponents.

Permeability is higher for linear length-aperture scaling as fractures contribute significantly to flow, illustrated by the heterogeneous fluid pressure contour lines (Figure 8e). This increase is mainly linked to several large fractures in the east of the model (Figures 8b and 8e). The average increase in permeability in all pavements is 123% in the direction parallel to σ_1 (the y direction) and 28% in the perpendicular direction (x direction) for linear length-aperture scaling (Table 2). Flow calculated from sublinear scaling shows similar increases.

4.1.2. Peak Shearing Criterion

The permeability increase resulting from the Barton-Bandis peak shear method is two times higher than matrix permeability (Figure 8f and Table 2). The contribution of fractures to flow within a single outcrop is relatively uniform; i.e., the increase in flow is the result of contributions from many fractures with a relatively small aperture, but with a high degree of connectivity, as indicated by the fluid pressure contour lines (Figure 8f). The fluid velocity is also relatively high and heterogeneous (Figure 8i).

4.1.3. Comparison of Flow Patterns: Coulomb Versus Peak Shear

Overall, Barton-Bandis peak shearing predicts the highest permeability in critically stressed networks in x and y directions (Table 2). This high impact on flow is not explained by the aperture distributions, as the average aperture of Barton-Bandis is 26 times smaller compared to linear length-aperture scaling. Instead, the high permeability is related to intrafracture connectivity, which we define as the connectivity along a single fracture. This is different from interfracture connectivity, which we define as the connectivity related to the spatial distribution of the network, including length, orientation, and spacing.

The impact of interfracture connectivity is best studied using percolation theory [*Mourzenko et al.*, 2011a, 2011b; *Sævik et al.*, 2013]. However, in each of the seven studied networks, interfracture connectivity, defined by the percolation parameters in Table 1, does not change, as only aperture is changed whereas length and spacing remain constant. Intrafracture connectivity does vary with each aperture model, as sections along a single fracture can be hydraulically closed depending on the critical stress model, forming aperture bottlenecks that affect intrafracture connectivity. In the Barton-Bandis model, the percolation parameter as defined by *Robinson* [1983] is 1.2, which is relatively close to the interfracture connectivity when all fractures are assumed open (1.7, Table 1). This indicates a low number of flow bottlenecks. The percolation probability of the linear length-aperture and power law methods is significantly lower, corresponding to a larger amount of flow bottlenecks (Figures 8d and 8e).

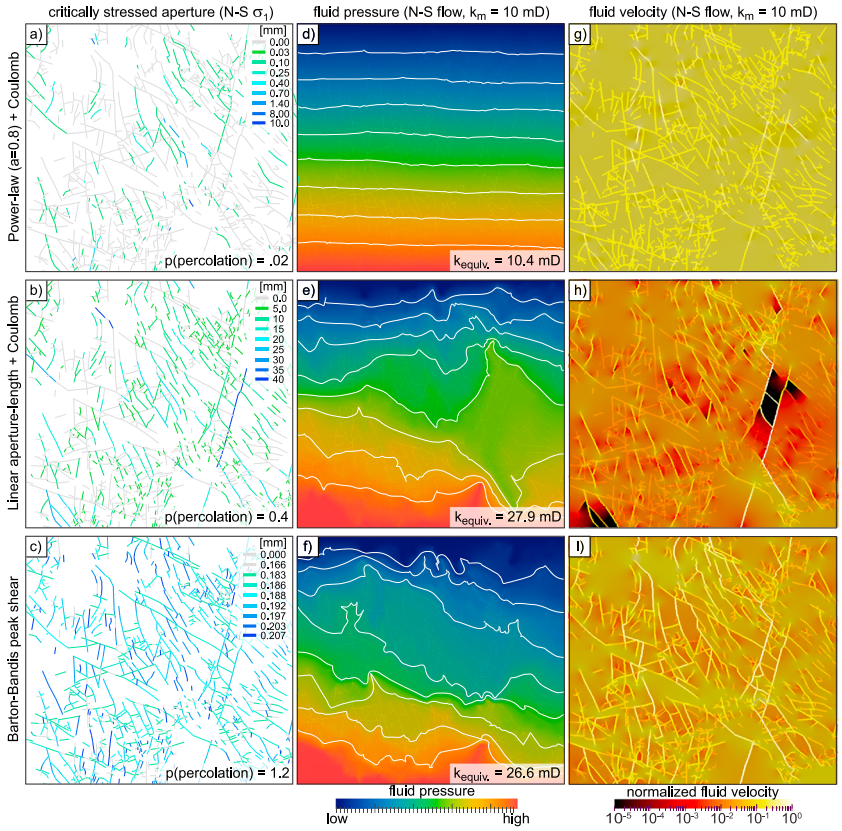

Figure 8. Critically stressed aperture distribution and subsequent fluid pressure distribution for the three main aperture methods, applied to pavement Brazil III. Critical stress analysis assumes a N-S maximum horizontal stress: (a) Critically stressed aperture for power law aperture scaling with an exponent of 0.8; (b) aperture as a function of length, using total fracture length; and (c) Barton-Bandis aperture distribution. The percolation probability as defined by [*Robinson*, 1983, 1984] for each aperture model is shown in the inset of the aperture distributions. The percolation probability of the entire network, assuming that all fractures are open, is 1.7; (d–f) N-S fluid pressure distributions for the critically stressed aperture distributions from Figures 8a–8c, modeled in a 10 mD matrix. White lines are fluid pressure contour lines. The resulting equivalent aperture is listed in each image; (g–i) N-S fluid velocity magnitude field, showing which fractures contribute most to the increase in effective permeability.

We plot the fluid velocities for each model to analyze which sections of the fracture network contribute most to flow (Figures 8g–8i). The fluid velocities indicate that the increase in permeability for linear length-aperture scaling is mainly the result of flow through several large fractures, in an otherwise poorly connected network of open fractures (Figures 8b and 8e), whereas for Barton-Bandis, most fractures are open, albeit with small aperture values (Figures 8c and 8f).

4.2. Impact of Matrix Permeability

The impact of intrafracture connectivity on permeability is observed for models with a 10 mD matrix permeability, but results change with changing matrix permeabilities. We quantify equivalent permeability resulting from matrix permeabilities between 1 mD and 1 darcy (Figure 9).

4.2.1. Coulomb Criterion

The relative contribution of fractures decreases for increasing matrix permeability when using power law aperture-frequency scaling with the Coulomb criterion (Figure 9a). In a low-permeability matrix (i.e., 1 mD), fractures increase permeability up to 60%, but for increasing matrix permeability, the impact of fractures decreases rapidly (Figure 9a). The rate of decrease for each pavement is different, and scales with fracture intensity.

Equivalent permeability is up to four times higher compared to matrix permeability for apertures resulting from the linear length scaling method and does not change for increasing matrix permeability up to 1 darcy.

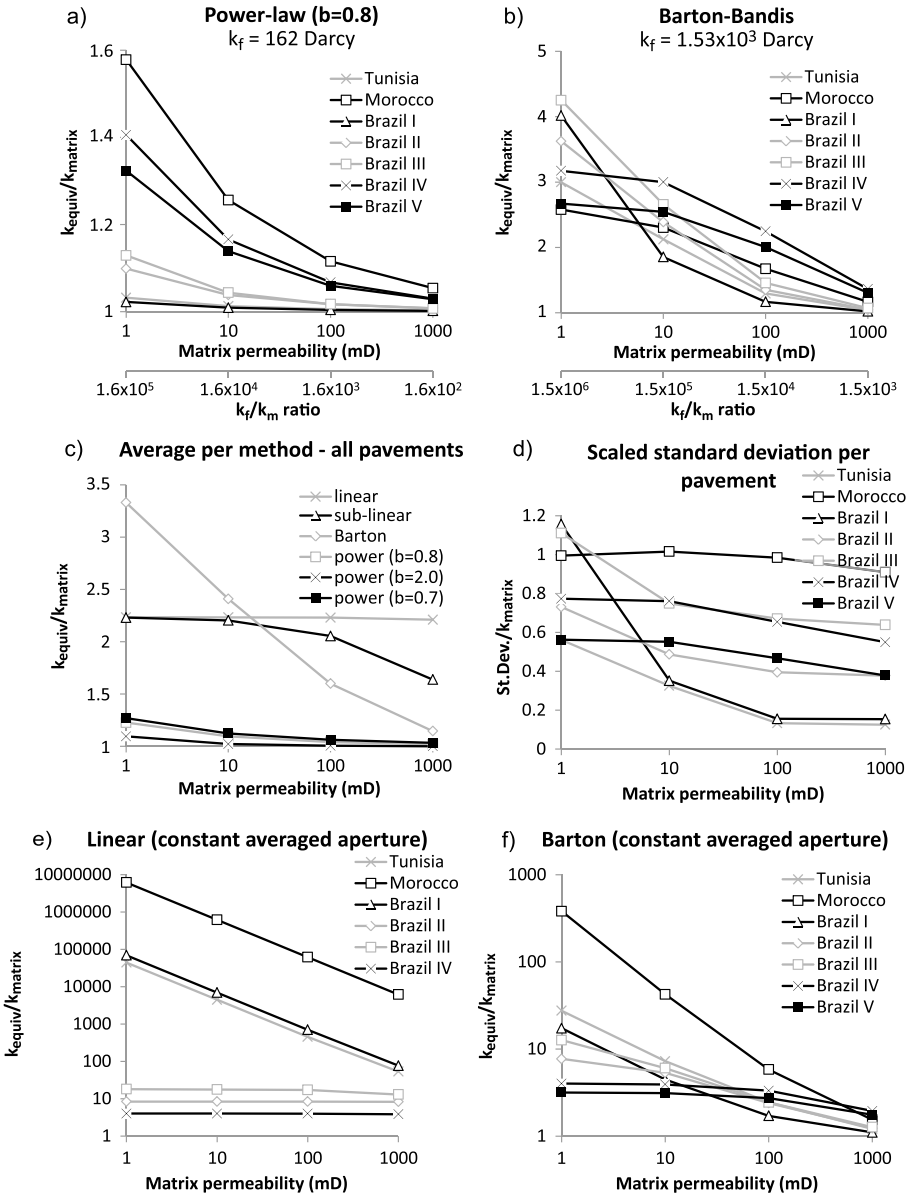

Figure 9. The impact of fracture permeability on equivalent permeability for a range of matrix permeabilities, plotted for all pavements using (a) power law and (b) Barton-Bandis apertures; (c) comparison of all aperture methods, averaged for all pavements; (d) standard deviation of the equivalent permeability for each pavement, averaged for all permeability models of each pavement. The average fracture permeability k_f, calculated for all critically stressed segments and weighted for the ratio of open segments, is listed in darcy in Figures 9a–9c, in addition to the ratio between k_f and k_m; averaging the heterogeneous aperture distributions to single values that are assigned to the entire fracture network results in a significantly larger contrast between equivalent and matrix permeability for (e) linear length-aperture scaling and (f) Barton-Bandis aperture.

This constant trend results from the large contrast between matrix and fracture, as the intrinsic fracture permeability is 2.1×10^6 darcy. The relative impact of fractures on permeability in the different pavements is a function of fracture intensity.

4.2.2. Peak Shearing Criterion

The average intrinsic fracture permeability of the Barton-Bandis distribution is 1.5×10^3 darcy, which is sufficiently high to create a large contrast between matrix and fracture flow for a low permeability, but for a 1 darcy matrix, the contrast, and hence the impact of fractures on permeability, is small (Figure 9b).

This trend is different depending on the fraction of critically stressed fractures, which controls intrafracture connectivity. Where intrafracture connectivity is high, the permeability increase is relatively low for high matrix permeabilities but increases for an impermeable matrix as fracture flow is not limited by intrafracture connectivity (Brazil I–III and Tunisia in Figure 9b). Fractures in the other pavements have a smaller impact in an impermeable matrix, as connectivity is lower.

4.2.3. Comparison of Fracture-Matrix Flow Contrasts

In a 10 mD matrix, Barton-Bandis peak shearing predicts the highest increase in permeability, compared to aperture-frequency and (sub)linear length-aperture scaling, based on the average of all pavements (Table 2). However, this only holds when matrix permeability is low, i.e., less than 20 mD (Figure 9c). For higher matrix permeabilities, the relative impact of Barton-Bandis on flow decreases, whereas the impact of (sub)linear scaling remains constant. The contribution of aperture-frequency scaling to permeability is low, irrespective of the power law exponent or matrix permeability.

5. Discussion

The models indicate that equivalent permeability varies depending on the aperture model and the contrast between fracture and matrix permeability. However, reservoir-scale flow models typically model equivalent permeability by upscaling fractures with a constant aperture. Although modeling of explicit fractures with varying apertures is not trivial on the scale of a reservoir model, some general observations can be derived from the presented 2-D models that may better capture the natural variability of fracture flow in upscaled models.

5.1. Impact of Intrafracture Connectivity

In all networks, the standard deviation for equivalent permeability is relatively large, resulting from the wide scatter in aperture predicted by the different methods (Figure 9d). However, the total increase in equivalent permeability compared to the matrix is relatively small compared to what is commonly observed in equivalent permeability models [e.g., *Jonoud and Jackson*, 2008; *Cottereau et al*., 2010]. This small increase is related to the heterogeneous aperture distribution, which includes 20–50% hydraulically closed fracture segments. These closed segments have a strong impact on flow, especially when matrix permeability is low.

To quantify the impact of using heterogeneous apertures, we calculate the average aperture for the linear scaling and Barton-Bandis methods and apply this as a constant aperture for the entire fracture network (Figures 9e and 9f). The ratio between equivalent and matrix permeability is higher for the models with a constant averaged aperture than for the heterogeneous distributions. Outcrop data indicate that a heterogeneous aperture is likely more representative than an averaged constant aperture [e.g., *Hooker et al*., 2009].

In 3-D, particularly when fractures are not vertical but have a scattered dip angle, the impact of closed segments or small apertures on permeability will be smaller, and hence, 2-D models likely underestimate intrafracture connectivity compared to 3-D [*de Dreuzy et al*., 2012]. The exact relation between 2-D and 3-D is difficult to quantify, however, as the opening profile in the vertical dimension is variable, with small apertures at the top and bottom, and maximum aperture at the center. The 3-D roughness of fractures can be modeled mechanically [e.g., *Nejati et al*., 2016], but these methods are generally limited to several tens of fractures. In some cases, depending on network geometry, corrections can be applied to predict 3-D permeability using 2-D tracemaps [*Lang et al*., 2014].

5.2. Impact of Matrix Permeability

The impact of fracture flow depends on the contrast between fracture and matrix permeability. In all models, increasing matrix permeability decreases the relative contribution of fractures, although the matrix-fracture contrast depends on the used aperture method. *Matthäi and Belayneh* [2004] used a similar approach to identify three characteristic flow regimes, defined by the ratio between intrinsic fracture permeability k_f and matrix permeability k_m, based on a 44 m^2 pavement model with two sets of natural fractures, each with a constant but different aperture, and fracture porosities similar to the values in this study. For a k_f/k_m ratio smaller than 10^2 they found that fractures have a negligible impact on permeability. For a ratio exceeding 10^3–10^4, fractures strongly perturb flow, and fractures carry all flow once the ratio exceeds 10^5–10^6. The transition between the latter two regimes is not analyzed in our study, but we do identify when fractures contribute significantly to permeability (Figures 9a and 9b). Our studied pavements are significantly larger than the 44 m^2 pavement model studied in *Matthäi and Belayneh* [2004].

We find the lowest ratios for the aperture-frequency and Barton-Bandis methods with a matrix permeability of 100 mD to 1 darcy, with a k_f/k_m ratio between 10^2 and 10^3. Depending on network geometry, the impact of fractures is negligible for some of the pavements, corresponding to what was found by *Matthäi and Belayneh* [2004].

The ratio for linear length-aperture scaling exceeds 10^6, even for a matrix permeability of 1 darcy, and fractures in these models contribute significantly to permeability, irrespective of fracture geometry. These models fall in the third category as defined by *Matthäi and Belayneh* [2004]. The ratio for power law aperture-frequency scaling does not correspond to the predicted flow domains, as the contribution of these apertures to permeability is low, irrespective of matrix permeability.

These ratios alone may not be sufficient to characterize flow regimes, as fracture network geometry and aperture-dependent intrafracture connectivity have a strong impact on permeability, especially for power law aperture-frequency scaling. Fractures contribute significantly to permeability in three of the pavements for a k_f/k_m ratio of 1.6×10^5, but for the same ratio, fracture flow is negligible in the Brazil I and Tunisia pavements (Figure 9a).

6. Conclusions

We have analyzed the impact of three fundamentally different methods to predict kinematic aperture and two critical stress criteria on permeability in naturally fractured reservoirs. The aperture models are based on the following: (i) power law aperture-frequency scaling observed in outcrops, (ii) (sub)linear length-aperture scaling resulting from Linear Elastic Fracture Mechanics, and (iii) Barton-Bandis shear-induced dilation. For the first two methods, critically stressed fractures are identified using a Coulomb criterion, whereas for the Barton-Bandis model, a peak shear criterion is used. These aperture and critical stress models are applied to seven deterministic fracture systems, digitized from outcropping fractured pavements in Brazil, Tunisia, and Morocco. The impact on permeability is quantified using combined fracture-matrix flow models, taking into account the heterogeneous aperture distributions and different matrix permeabilities. The main findings derived from these models are the following:

1. Linear length-aperture scaling predicts the largest kinematic apertures. Sublinear aperture, although based on similar principles, is two to eight times smaller, depending on fracture length. Barton-Bandis aperture is smaller and limited to a narrow domain, depending on mechanical properties and the applied stress conditions. The smallest apertures result from power law frequency scaling and decrease for increasing power law exponents.
2. The Barton-Bandis peak shearing criterion predicts that on average, 80% of the fractures in the studied networks are critically stressed. For the same conditions, the Coulomb criterion predicts that 50% is critically stressed. This difference is related to nonlinear fracture behavior, which is considered by the Barton-Bandis method by incorporating length and spacing into the critical stress analysis, but not by the Coulomb method.
3. We find consistent relative trends between the different aperture methods, which are partially related to network geometry. Power law scaling is only a function of intensity, resulting in an equivalent permeability that is strongly related to fracture intensity (Table 1 and Figure 9). For (sub)linear length-aperture scaling, intensity is not representative of permeability, as it does not distinguish between long and short fractures, but length-weighted intensity does capture permeability trends. For Barton-Bandis, the relation between geometry and permeability is less straight forward, as aperture in this model is also a function of roughness, which changes nonlinearly as a function of stress.
4. The impact of each aperture and critical stress method on permeability depends on matrix permeability. For a low-permeability matrix, permeability is highest in networks that have a high ratio of critically stressed fractures, i.e., high intrafracture connectivity, irrespective of the absolute aperture values. In this case, critically stressed aperture derived from Barton-Bandis peak shearing has the largest impact on flow. For a higher-permeability matrix, flow bottlenecks formed by zero-aperture segments are bypassed through the permeable matrix, and models with large aperture values such as (sub)linear length-aperture scaling predict the highest equivalent permeability, even if the fracture network is disconnected.
5. Different flow regimes can be identified based on the k_f/k_m ratio, similar to what is observed by *Matthäi and Belayneh* [2004], but the exact transition between the different domains also depends on fracture network geometry. Furthermore, power law aperture-frequency scaling does not fit the defined flow regimes, as fractures contribute little to permeability even when the k_f/k_m ratio is high.

Acknowledgments

The authors thank TOTAL SA for financial support of the PhD research of the first author and for permitting publication of the results. We specifically thank B. Gauthier, A. Kamp, and Y. Leroy from TOTAL SA for fruitful discussions. The outcropping fracture networks have been acquired and interpreted with help from F. H. Bezerra (UFRN, Brazil), S. Bouaziz and A. Hammami (ENIS, Tunisia), H. Boro, M. van Eijk, K. Ewondo, J. van der Vaart, R. Vaughan and E. van der Voet (VU University Amsterdam, Netherlands), and K. Althuis (TU Delft, Netherlands). Data acquisition in Brazil was partly sponsored by Agência Nacional de Petróleo (ANP, Brazilian Agency of Petroleum) and Petrobras. N. J. Hardebol is thanked for supplying DigiFract software for fracture interpretation and for productive discussions regarding the aperture models. We thank Golder Associates for supplying FracMan software, used for fracture cluster analysis. The fracture data used in this study are published in part in the 3TU repository: http://data.3tu.nl/repository/uuid:be07fe95-417c-44e9-8c6a-d13f186abfbb and http://data.3tu.nl/repository/uuid:6d096e88-14e0-4d6e-aeca-a0b9f7b3ea56. The Morocco fracture data are available from the second author. We thank the Editor P. Tregoning and two anonymous reviewers for their constructive reviews and feedback that significantly improved the initial manuscript.

References

Anders, M. H., S. E. Laubach, and C. H. Scholz (2014), Microfractures: A review, *J. Struct. Geol.*, doi:10.1016/j.jsg.2014.05.011.

Atkinson, B. K. (1984), Subcritical crack growth in geological materials, *J. Geophys. Res.*, *89*(B6), 4077–4114, doi:10.1029/JB089iB06p04077.

Baghbanan, A., and L. Jing (2008), Stress effects on permeability in a fractured rock mass with correlated fracture length and aperture, *Int. J. Rock Mech. Min. Sci.*, *45*(8), 1320–1334, doi:10.1016/j.ijrmms.2008.01.015.

Bandis, S. C., A. C. Lumsden, and N. R. Barton (1983), Fundamentals of rock joint deformation, *Int. J. Rock Mech. Min. Sci. Geomech. Abstr.*, *20*(6), 249–268, doi:10.1016/0148-9062(83)90595-8.

Barton, C. A., M. D. Zoback, and D. Moos (1995), Fluid flow along potentially active faults in crystalline rock, *Geology*, *23*(8), 683–686, doi:10.1130/0091-7613(1995)023<0683:FFAPAF>2.3.CO;2.

Barton, N. (1982), *Modelling Rock Joint Behaviour From In Situ Block Tests: Implications for Nuclear Waste Repository Design*, Office of Nuclear Waste Isolation, Columbus, Ohio.

Barton, N. (2014), Non-linear behaviour for naturally fractured carbonates and frac-stimulated gas-shales, *First Break*, *32*(2031), 51–66, doi:10.3997/1365-2397.2014011.

Barton, N., and S. Bandis (1980), Some effects of scale on the shear strength of joints, in *International Journal of Rock Mechanics and Mining Sciences & Geomechanics Abstracts*, vol. 17, pp. 69–73, Pergamon Press.

Barton, N., S. Bandis, and K. Bakhtar (1985), Strength, deformation and conductivity coupling of rock joints, *Int. J. Rock Mech. Min. Sci. Geomech. Abstr.*, *22*(3), 121–140, doi:10.1016/0148-9062(85)93227-9.

Belayneh, M., S. Geiger, and S. K. Matthäi (2006), Numerical simulation of water injection into layered fractured carbonate reservoir analogs, *Am. Assoc. Petrol. Geol. Bull.*, *90*(10), 1473–1493, doi:10.1306/05090605153.

Berkowitz, B. (1995), Analysis of fracture network connectivity using percolation theory, *Math. Geol.*, *27*(4), 467–483, doi:10.1007/BF02084422.

Berkowitz, B., and I. Balberg (1993), Percolation theory and its application to groundwater hydrology, *Water Resour. Res.*, *29*(4), 775–794, doi:10.1029/92WR02707.

Bertotti, G., and K. Bisdom (2013), *Fracture Patterns in the Jandaira Fm. (NE Brazil)*, Delft Univ. of Technology, Delft, doi:10.4121/uuid:be07fe95-417c-44e9-8c6a-d13f186abfbb.

Bertotti, G., F. H. R. Bezerra, K. Bisdom, C. L. Cazarin, and J. Reijmer (2013), Outcropping analogs and multiscale fracture patterns in the Jandaíra Formation First EAGE/SBGf Work. 2013 Fract. Conv. Unconv. Reserv. 5-6 Novemb. 2013, Copacabana, Rio Janeiro, Brazil, (November 2013), 5–7.

Bisdom, K. (2015), *Natural Fracture Patterns in Carbonate Rocks*, Delft Univ. of Technology, Delft, doi:10.4121/uuid:6d096e88-14e0-4d6e-aeca-a0b9f7b3ea56.

Bisdom, K., G. Bertotti, and H. M. Nick (2016a), A geometrically based method for predicting stress-induced fracture aperture and flow in discrete fracture networks, *Am. Assoc. Petrol. Geol. Bull.*, doi:10.1306/02111615127.

Bisdom, K., G. Bertotti, and H. M. Nick (2016b), The impact of in-situ stress and outcrop-based fracture geometry on hydraulic aperture and upscaled permeability in fractured reservoirs, *Tectonophysics*, doi:10.1016/j.tecto.2016.04.006.

Bonnet, E., O. Bour, N. E. Odling, P. Davy, I. Main, P. Cowie, and B. Berkowitz (2001), Scaling of fracture systems in geological media, *Rev. Geophys.*, *39*(3), 347–383, doi:10.1029/1999RG000074.

Cottereau, N., M. H. Garcia, O. R. Gosselin, and L. Vigier (2010), Effective fracture network permeability: Comparative study of calculation methods, *SPE Eur. Annu. Conf. Exhib.*, doi:10.2118/131126-ms.

de Dreuzy, J. R., P. Davy, and O. Bour (2001), Hydraulic properties of two-dimensional random fracture networks following a power law length distribution: 2. Permeability of networks based on lognormal distribution of apertures, *Water Resour. Res.*, *37*(8), 2079–2095, doi:10.1029/2001WR900010.

de Dreuzy, J.-R., P. Davy, and O. Bour (2002), Hydraulic properties of two-dimensional random fracture networks following power law distributions of length and aperture, *Water Resour. Res.*, *38*(12), 1276, doi:10.1029/2001WR001009.

de Dreuzy, J.-R., Y. Méheust, and G. Pichot (2012), Influence of fracture scale heterogeneity on the flow properties of three-dimensional discrete fracture networks (DFN), *J. Geophys. Res.*, *117*, B11207, doi:10.1029/2012JB009461.

Dershowitz, W. S., and H. H. Einstein (1988), Characterizing rock joint geometry with joint system models, *Rock Mech. Rock Eng.*, *51*(1), 21–51, doi:10.1007/BF01019674.

Engelder, T., and A. Lacazette (1990), Natural hydraulic fracturing, in *Rock Joints*, edited by N. Barton and O. Stephansson, pp. 35–44, Balkema, Rotterdam.

Gale, J. F. W., S. E. Laubach, J. E. Olson, P. Eichhuble, and A. Fall (2014), Natural fractures in shale: A review and new observations, *Am. Assoc. Petrol. Geol. Bull.*, *98*(11), 2165–2216, doi:10.1306/08121413151.

Guiton, M. L. E., W. Sassi, Y. M. Leroy, and B. D. M. Gauthier (2003), Mechanical constraints on the chronology of fracture activation in folded Devonian sandstone of the western Moroccan Anti-Atlas, *J. Struct. Geol.*, *25*, 1317–1330, doi:10.1016/S0191-8141(02)00155-4.

Hardebol, N. J., and G. Bertotti (2013), DigiFract: A software and data model implementation for flexible acquisition and processing of fracture data from outcrops, *Comput. Geosci.*, *54*, 326–336, doi:10.1016/j.cageo.2012.10.021.

Hooker, J. N., J. F. W. Gale, L. A. Gomez, S. E. Laubach, R. Marrett, and R. M. Reed (2009), Aperture-size scaling variations in a low-strain opening-mode fracture set, Cozzette Sandstone, Colorado, *J. Struct. Geol.*, *31*(7), 707–718, doi:10.1016/j.jsg.2009.04.001.

Hooker, J. N., L. A. Gomez, S. E. Laubach, J. F. W. Gale, and R. Marrett (2012), Effects of diagenesis (cement precipitation) during fracture opening on fracture aperture-size scaling in carbonate rocks, *Geol. Soc. London, Spec. Publ.*, *370*(1), 187–206, doi:10.1144/SP370.9.

Hooker, J. N., S. E. Laubach, and R. Marrett (2013), Fracture-aperture size—Frequency, spatial distribution, and growth processes in strata-bounded and non-strata-bounded fractures, Cambrian Mesón Group, NW Argentina, *J. Struct. Geol.*, *54*, 54–71, doi:10.1016/j.jsg.2013.06.011.

Hooker, J. N., S. E. Laubach, and R. Marrett (2014), A universal power-law scaling exponent for fracture apertures in sandstones, *Geol. Soc. Am. Bull.*, *126*(9-10), 1340–1362, doi:10.1130/B30945.1.

Jonoud, S., and M. Jackson (2008), Validity of steady-state upscaling techniques, *SPE Reservoir Eval. Eng.*, *11*(2), 12–15, doi:10.2118/100293-PA.

Klimczak, C., R. A. Schultz, R. Parashar, and D. M. Reeves (2010), Cubic law with aperture-length correlation: Implications for network scale fluid flow, *Hydrogeol. J.*, *18*(4), 851–862, doi:10.1007/s10040-009-0572-6.

Lang, P. S., A. Paluszny, and R. W. Zimmerman (2014), Permeability tensor of three-dimensional fractured porous rock and a comparison to trace map predictions, *J. Geophys. Res. Solid Earth*, *119*, 6288–6307, doi:10.1002/2014JB011027.

Laubach, S. E., and M. E. Ward (2006), Diagenesis in porosity evolution of opening-mode fractures, Middle Triassic to Lower Jurassic La Boca Formation, NE Mexico, *Tectonophysics*, *419*(1-4), 75–97, doi:10.1016/j.tecto.2006.03.020.

Laubach, S. E., J. E. Olson, and J. F. Gale (2004), Are open fractures necessarily aligned with maximum horizontal stress?, *Earth Planet. Sci. Lett.*, *222*(1), 191–195, doi:10.1016/j.epsl.2004.02.019.
Lawn, B. R., and T. R. Wilshaw (1975), *Fracture of Brittle Solids*, Cambridge Univ. Press, Cambridge, U. K.
Lei, Q., J.-P. Latham, J. Xiang, C.-F. Tsang, P. Lang, and L. Guo (2014), Effects of geomechanical changes on the validity of a discrete fracture network representation of a realistic two-dimensional fractured rock, *Int. J. Rock Mech. Min. Sci.*, *70*, 507–523, doi:10.1016/j.ijrmms.2014.06.001.
Lei, Q., J. Latham, C. Tsang, J. Xiang, and P. Lang (2015), A new approach to upscaling fracture network models while preserving geostatistical and geomechanical characteristics, *J. Geophys. Res. Solid Earth*, *120*, 4784–4807, doi:10.1002/2014JB011736.
Lorenz, J. C., L. W. Teufel, and N. R. Warpinski (1991), Regional fractures I: A mechanism for the formation of regional fractures at depth in flat-lying reservoirs, *Am. Assoc. Petrol. Geol. Bull.*, *75*(11), 1714–1737, doi:10.1306/0C9B29E3-1710-11D7-8645000102C1865D.
Luthi, S. M., and P. Souhaite (1990), Fracture apertures from electrical borehole scans, *Geophysics*, *55*(7), 821–833, doi:10.1190/1.1442896.
Makel, G. H. (2007), The modelling of fractured reservoirs: Constraints and potential for fracture network geometry and hydraulics analysis, *Geol. Soc. London, Spec. Publ.*, *292*(1), 375–403, doi:10.1144/SP292.21.
Marrett, R., O. J. Ortega, and C. M. Kelsey (1999), Extent of power-law scaling for natural fractures in rock, *Geology*, *27*(9), 799–802, doi:10.1130/0091-7613(1999)027<0799:EOPLSF>2.3.CO;2.
Matthäi, S. K., and H. M. Nick (2009), Upscaling two-phase flow in naturally fractured reservoirs, *Am. Assoc. Pet. Geol. Bull.*, *93*(11), 1621–1632, doi:10.1306/08030909085.
Matthäi, S. K., and M. Belayneh (2004), Fluid flow partitioning between fractures and a permeable rock matrix, *Geophys. Res. Lett.*, *31*, L07602, doi:10.1029/2003GL019027.
Matthäi, S. K., H. M. Nick, C. Pain, and I. Neuweiler (2009), Simulation of solute transport through fractured rock: A higher-order accurate finite-element finite-volume method permitting large time steps, *Transp. Porous Media*, *83*(2), 289–318, doi:10.1007/s11242-009-9440-z.
Matthäi, S., A. Mezentsev, and M. Belayneh (2007), Finite element—Node-centered finite-volume two-phase-flow experiments with fractured rock represented by unstructured hybrid-element meshes, SPE Reserv. Eval. Eng., 10(December), doi:10.2118/93341-PA.
Moos, D., and C. Barton (2008), Modeling uncertainty in the permeability of stress-sensitive fractures 42nd US Rock Mech. Symp., ARMA 08-31.
Mourzenko, V. V., J. F. Thovert, and P. M. Adler (2011a), Permeability of isotropic and anisotropic fracture networks, from the percolation threshold to very large densities, *Phys. Rev. E - Stat. Nonlinear, Soft Matter Phys.*, *84*(3), 1–20, doi:10.1103/PhysRevE.84.036307.
Mourzenko, V. V., J. F. Thovert, and P. M. Adler (2011b), Trace analysis for fracture networks with anisotropic orientations and heterogeneous distributions, *Phys. Rev. E - Stat. Nonlinear, Soft Matter Phys.*, *83*(3), 1–18, doi:10.1103/PhysRevE.83.031104.
Narr, W. (1996), Estimating average fracture spacing in subsurface rock, *Am. Assoc. Petrol. Geol. Bull.*, *80*(10), 1565–1586.
Narr, W., D. S. Schechter, and L. B. Thompson (2006), *Naturally Fractured Reservoir Characterization*, Soc. of Petrol. Eng., Richardson, Tex.
Nejati, M., A. Paluszny, and R. W. Zimmerman (2016), A finite element framework for modeling internal frictional contact in three-dimensional fractured media using unstructured tetrahedral meshes, *Comput. Methods Appl. Mech. Eng.*, doi:10.1016/j.cma.2016.03.028.
Nelson, R. A. (2001), *Geologic Analysis of Naturally Fractured Reservoirs*, 2nd ed., Gulf Prof., Woburn.
Nick, H. M., and S. K. Matthäi (2011), Comparison of three FE-FV numerical schemes for single- and two-phase flow simulation of fractured porous media, *Transp. Porous Media*, *90*(2), 421–444, doi:10.1007/s11242-011-9793-y.
Nick, H. M., A. Paluszny, M. J. Blunt, and S. K. Matthäi (2011), Role of geomechanically grown fractures on dispersive transport in heterogeneous geological formations, *Phys. Rev. E*, *84*(5056301), doi:10.1103/PhysRevE.84.056301.
Odling, N. E., et al. (1999), Variations in fracture system geometry and their implications for fluid flow in fractures hydrocarbon reservoirs, *Pet. Geosci.*, *5*(4), 373–384, doi:10.1144/petgeo.5.4.373.
Olson, J. E. (2003), Sublinear scaling of fracture aperture versus length: An exception or the rule?, *J. Geophys. Res.*, *108*(B9), 2413, doi:10.1029/2001JB000419.
Olson, J. E., and R. A. Schultz (2011), Comment on "A note on the scaling relations for opening mode fractures in rock" by C.H. Scholz, *J. Struct. Geol.*, *33*(10), 1523–1524, doi:10.1016/j.jsg.2011.07.004.
Olson, J. E., S. E. Laubach, and R. H. Lander (2009), Natural fracture characterization in tight gas sandstones: Integrating mechanics and diagenesis, *Am. Assoc. Petrol. Geol. Bull.*, *93*(11), 1535–1549, doi:10.1306/08110909100.
Olsson, R., and N. Barton (2001), An improved model for hydromechanical coupling during shearing of rock joints, *Int. J. Rock Mech. Min. Sci.*, *38*(3), 317–329, doi:10.1016/S1365-1609(00)00079-4.
Ortega, O. J., R. A. Marrett, and S. E. Laubach (2006), A scale-independent approach to fracture intensity and average spacing measurement, *Am. Assoc. Petrol. Geol. Bull.*, *90*(2), 193–208, doi:10.1306/08250505059.
Paluszny, A., and S. K. Matthäi (2010), Impact of fracture development on the effective permeability of porous rocks as determined by 2-D discrete fracture growth modeling, *J. Geophys. Res.*, *115*, B02203, doi:10.1029/2008JB006236.
Philip, Z. G., J. W. Jennings, J. E. Olson, S. E. Laubach, and J. Holder (2005), Modeling coupled fracture-matrix fluid flow in geomechanically simulated fracture networks, *SPE Reserv. Eval. Eng.*, *8*(04), 300–309, doi:10.2118/77340-PA.
Pollard, D. D., and P. Segall (1987), Theoretical displacements and stresses near fractures in rock: With applications to faults, veins, dikes, and solution surfaces, in *Fracture Mechanics of Rock*, pp. 277–349 , Elsevier, Berlin, Heidelberg.
Ponziani, M., E. Slob, S. Luthi, R. Bloemenkamp, and I. Le Nir (2015), Experimental validation of fracture aperture determination from borehole electric microresistivity measurements, *Geophysics*, *80*(3), D175–D181, doi:10.1190/geo2014-0334.1.
Reis, Á. F. C., F. H. R. Bezerra, J. M. Ferreira, A. F. Do Nascimento, and C. C. Lima (2013), Stress magnitude and orientation in the Potiguar Basin, Brazil: Implications on faulting style and reactivation, *J. Geophys. Res. Solid Earth*, *118*, 5550–5563, doi:10.1002/2012JB009953.
Riley, P., C. Gordon, J. A. Simo, B. Tikoff, and M. Soussi (2010), Structure of the Alima and associated anticlines in the foreland basin of the southern Atlas Mountains, Tunisia, *Lithosphere*, *3*(1), 76–91, doi:10.1130/L119.1.
Robinson, P. C. (1983), Connectivity of fracture systems-a percolation theory approach, *J. Phys. A: Math. Gen.*, *16*(3), 605–614, doi:10.1088/0305-4470/16/3/020.
Robinson, P. C. (1984), Numerical calculations of critical densities for lines and planes, *J. Phys. A: Math. Gen.*, *17*(14), 2823–2830, doi:10.1088/0305-4470/17/14/025.
Rogers, S. F. (2003), Critical stress-related permeability in fractured rocks, *Geol. Soc. London, Spec. Publ.*, *209*(1), 7–16, doi:10.1144/GSL.SP.2003.209.01.02.
Sævik, P. N., I. Berre, M. Jakobsen, and M. Lien (2013), A 3D computational study of effective medium methods applied to fractured media, *Transp. Porous Media*, *100*(1), 115–142, doi:10.1007/s11242-013-0208-0.
Scholz, C. H. (2010), A note on the scaling relations for opening mode fractures in rock, *J. Struct. Geol.*, *32*(10), 1485–1487, doi:10.1016/j.jsg.2010.09.007.
Scholz, C. H. (2011), Reply to comments of Jon Olson and Richard Schultz, *J. Struct. Geol.*, *33*(10), 1525–1526, doi:10.1016/j.jsg.2011.07.006.

Schultz, R. A., C. Klimczak, H. Fossen, J. E. Olson, U. Exner, D. M. Reeves, and R. Soliva (2013), Statistical tests of scaling relationships for geologic structures, *J. Struct. Geol.*, *48*, 85–94, doi:10.1016/j.jsg.2012.12.005.

Segall, P. (1984), Formation and growth of extensional fracture sets, *Geol. Soc. Am. Bull.*, *95*(4), 454–462, doi:10.1130/0016-7606(1984)95<454:FAGOEF>2.0.CO;2.

Segall, P., and D. D. Pollard (1983), Joint formation in granitic rock of the Sierra Nevada, *Geol. Soc. Am. Bull.*, *94*(5), 563–575, doi:10.1130/0016-7606(1983)94<563:JFIGRO>2.0.CO;2.

Snow, D. T. (1969), Anisotropic permeability of fractured media, *Water Resour. Res.*, *5*(6), 1273–1289, doi:10.1029/WR005i006p01273.

Swarbrick, R. E., M. J. Osborne, and G. S. Yardley (2002), Comparison of overpressure magnitude resulting from the main generating mechanisms, *AAPG Mem.*, *76*, 1–12.

Tao, Q., C. A. Ehlig-Economides, and A. Ghassemi (2009), Investigation of stress-dependent permeability in naturally fractured reservoirs using a fully coupled poroelastic displacement discontinuity model, in *SPE Annual Technical Conference and Exhibition*, Soc. of Petrol. Eng., New Orleans, Louisiana.

Vermilye, J. M., and C. H. Scholz (1995), Relation between vein length and aperture, *J. Struct. Geol.*, *17*(3), 423–434, doi:10.1016/0191-8141(94)00058-8.

Wu, H. Q., and D. D. Pollard (2002), Imaging 3-D fracture networks around boreholes, *Am. Assoc. Petrol. Geol. Bull.*, *86*(4), 593–604, doi:10.1306/61EEDB52-173E-11D7-8645000102C1865D.

Zoback, M. D. (2007), *Reservoir Geomechanics*, Cambridge Univ. Press, Cambridge, U. K.